Received: 31 August 2020 | Revised: 19 March 2021 | Accepted: 25 March 2021

DOI: 10.1096/fj.202002028RR

RESEARCH ARTICLE

THE FASEB JOURNAL

Altered theta and beta oscillatory synchrony in a genetic mouse model of pathological anxiety

Hugo Cruces-Solis[1] | **Olga Babaev**[1,2] | **Heba Ali**[1,2] | **Carolina Piletti Chatain**[1,2] | **Vasyl Mykytiuk**[1,2] | **Nursen Balekoglu**[1] | **Sally Wenger**[1] | **Dilja Krueger-Burg**[1,3]

[1]Department of Molecular Neurobiology, Max Planck Institute of Experimental Medicine, Göttingen, Germany

[2]Göttingen Graduate School for Neurosciences, Biophysics, and Molecular Biosciences, University of Göttingen, Göttingen, Germany

[3]Department of Psychiatry and Psychotherapy, University Medical Center Göttingen, Göttingen, Germany

Correspondence
Dilja Krueger-Burg, Department of Psychiatry and Psychotherapy, University Medical Center Göttingen, Von-Siebold-Str. 5; 37075 Göttingen, Germany.
Email: dilja.krueger-burg@med.uni-goettingen.de

Funding information
Brain and Behavior Research Foundation (BBRF); Minerva Foundation (Minerva Stiftung); European Commission (EC)

Abstract

While the neural circuits mediating normal, adaptive defensive behaviors have been extensively studied, substantially less is currently known about the network mechanisms by which aberrant, pathological anxiety is encoded in the brain. Here we investigate in mice how deletion of Neuroligin-2 (Nlgn2), an inhibitory synapse-specific adhesion protein that has been associated with pathological anxiety and other psychiatric disorders, alters the communication between key brain regions involved in mediating defensive behaviors. To this end, we performed multi-site simultaneous local field potential (LFP) recordings from the basolateral amygdala (BLA), centromedial amygdala (CeM), bed nucleus of the stria terminalis (BNST), prefrontal cortex (mPFC) and ventral hippocampus (vHPC) in an open field paradigm. We found that LFP power in the vHPC was profoundly increased and was accompanied by an abnormal modulation of the synchrony of theta frequency oscillations particularly in the vHPC-mPFC-BLA circuit. Moreover, deletion of Nlgn2 increased beta and gamma frequency synchrony across the network, and this increase was associated with increased center avoidance. Local deletion of Nlgn2 in the vHPC and BLA revealed that they encode distinct aspects of this avoidance phenotype, with vHPC linked to immobility and BLA linked to a reduction in exploratory activity. Together, our data demonstrate that alterations in long-range functional connectivity link synaptic inhibition to abnormal defensive behaviors, and that both exaggerated activation of normal defensive circuits and recruitment of fundamentally distinct mechanisms contribute to this phenotype. *Nlgn2* knockout mice therefore represent a highly relevant model to study the role of inhibitory synaptic transmission in the circuits underlying anxiety disorders.

KEYWORDS
coherence, conditional, Cre, fear, GABA, neuroligin2, NL2

Abbreviations: BLA, basolateral amygdala; BNST, bed nucleus of the stria terminalis; CeM, centromedial amygdala; GABA, gamma-aminobutyric acid; LFP, local field potential; mPFC, medial prefrontal cortex; Nlgn2, Neuroligin-2; OF, open field; vHPC, ventral hippocampus.

Hugo Cruces-Solis and Olga Babaev contributed equally.

1 | INTRODUCTION

Anxiety disorders are among the most common psychiatric illnesses, affecting an estimated one in nine people in any given year and posing a significant burden for affected individuals, their families and society.[1,2] Pathological anxiety arises when normally adaptive defensive behaviors, such as avoidance of potentially threatening situations, become persistent, excessive and out of proportion to the actual threat posed, severely interfering with activities of daily life.[1-5] Understanding the biological mechanisms that underlie the transition from adaptive to pathological anxiety is therefore paramount in developing new treatment strategies for anxiety disorders in order to alleviate this burden.

One of the factors that contribute to the development of pathological anxiety behaviors are alterations in GABAergic inhibitory synaptic transmission.[6,7] Anxiolytic medications such as benzodiazepines target the GABAergic system, and variants in components of the molecular machinery at inhibitory synapses have been associated with anxiety disorders.[5-8] One of these components is Neuroligin-2 (Nlgn2), a postsynaptic adhesion protein that is localized selectively to inhibitory synapses[9-11] and that has been linked to anxiety disorders and co-morbid autism and schizophrenia.[12-14] Deletion of Nlgn2 in mice results in impaired inhibitory synaptic transmission in the hippocampus, amygdala and cortex[10,11,15-18] as well as a strongly exaggerated avoidance behavior in an anxiogenic environment.[17,19,20] These observations indicate that impaired inhibitory synaptic transmission in the *Nlgn2* knockout (KO) mice results in aberrant activation of the network mediating defensive behaviors, providing a unique opportunity to study the abnormal processing of anxiety-related information across the brain. In particular, we sought to determine whether these pathological defensive behaviors are encoded by the same mechanisms as adaptive behaviors and represent an excessive activation of the relevant circuits, or whether the etiological factors that result in anxiety disorders may fundamentally alter information processing in these circuits.

To address this question, we performed simultaneous multi-site local field potential (LFP) recordings in multiple brain regions in wildtype (WT) and *Nlgn2* KO mice under anxiogenic conditions in an open field (OF) paradigm. Specifically, we focused on five brain regions known to be essential for anxiety processing and the context-dependent regulation of defensive behaviors, including the basolateral amygdala (BLA), centromedial amygdala (CeM), ventral hippocampus (vHPC), medial prefrontal cortex (mPFC) and bed nucleus of stria terminalis (BNST).[4,21-30] Our data indicate that disruptions in synaptic inhibition due to loss of Nlgn2 result in both exaggerated activation of normal defensive circuits and recruitment of fundamentally distinct mechanisms, most notably alterations in long-range connectivity between brain regions, which in combination may encode the observed excessive avoidance behaviors.

2 | MATERIALS AND METHODS

2.1 | Animals

Nlgn2 KO mice[18] were maintained on a C57BL/6JRj background (Janvier Labs, Le Genest-Saint-Isle, France), and experimental groups consisted of male WT and KO littermates generated from heterozygous breeders at the Max Planck Institute of Experimental Medicine. *Nlgn2* conditional KO mice were generated in our laboratory (see below and Figure 5 for details) on a C57BL/6N background and were backcrossed onto a C57BL/6JRj background for at least six generations. For experiments, male homozygous cKO mice were generated from homozygous breeders. Mice were 8-12 weeks old at the beginning of the experiment. All animals were maintained on a 12 hours light/dark cycle (7 AM/7 PM), with food and water ad libitum, and all experiments were performed during the light cycle. The experimenter was blind to genotype during all stages of data acquisition and analysis. All procedures were approved by the State of Niedersachsen (Landesamt für Verbraucherschutz und Lebensmittelsicherheit) and were carried out in agreement with the guidelines for the welfare of experimental animals issued by the Federal Government of Germany and the Max Planck Society.

2.2 | Electrode implantation for in vivo electrophysiology

Mice received an intraperitoneal (i.p.) injection of Carprofen (5 mg/kg) to reduce post-surgery pain 30 minutes prior to surgery, and they were then anesthetized with Avertin (loading dose 20 mL/kg, maintenance dose 2 mL/kg i.p.). Anesthetized mice were placed in a digital stereotaxic frame and their body temperature was monitored by a rectal probe and maintained at 36°C. An incision in the midline of the scalp was made to expose the skull. Bregma and lambda were aligned to a plane level ± 50 µm. Prior to implantation, the tips of the electrodes were dipped in DiI (1,1′-Dioctadecyl-3,3,3′,3′-Tetramethylindocarbocyanine Perchlorate) for post-hoc histological verification. Electrodes were implanted individually into the right vHPC (−3.08 mm AP, 3.4 mm ML and −3.8 mm DV from brain surface), mPFC (2.1 mm AP, 0.4 mm ML and −1.4 DV), BLA (−1.22 mm AP, 3.15 mm ML and −4.3 mm DV), CeM (−1.22 mm AP, 2.3 mm ML and −5.04 mm DV) and BNST (−0.2 mm AP, 0.4 mm ML and −4.3 mm DV). The electrodes consisted of individual insulated tungsten wires (70 µm inner diameter) inserted into

a polymide tube (127 μm inner diameter) and attached to an 18-pin Omnetics connector (Omnetics, Minneapolis, MN, USA). A reference screw was implanted above the cerebellum. The implant was secured with three screws implanted in the skull and bonded with dental cement.

Immediately after the surgery, mice received subcutaneously analgesic (Carprofen 5 mg/kg) and antibiotic (Baytril 5 mg/kg). 24 hours after the surgery, mice received Carprofen (5 mg/kg) subcutaneously and Baytril in the drinking water (0.2 mg/mL). After surgery, mice were single-housed and were allowed to recover for seven days before behavioral analysis and data acquisition (see below). They were then sacrificed for histological verification of the recording site (Figure S1). For histological verification of the recording site, serial sections (40 μm) of the regions of interest were collected, stained for DAPI, mounted and cover slipped. The targeted brain region was identified in the section with the most ventral positive signal for DiI. In cases where the DiI signal could not be determined, we discarded the recordings from that electrode.

2.3 | In vivo electrophysiology data acquisition during OF behavior

OF behavior and in vivo electrophysiological recordings were performed after seven days of recovery. Mice were first habituated to the recording setup for four days, during which they were tethered to the acquisition system and recorded for five minutes in a habituation context (home cage with dim light ~30 lux). On the fifth day, mice were tethered to the system and recorded during five minutes in the habituation condition. Afterwards, the mice were placed into a wooden circular open field chamber (50 cm diameter) with a light intensity of 90 lux, and they were permitted to explore the chamber for 15 minutes. Between each mouse, the arena was cleaned thoroughly with 70% ethanol followed by water to eliminate any odors left by the previous mouse.

Electrophysiological signals were amplified, digitized, multiplexed and sent to the acquisition board, a RHD2132 16-channel amplifier board (Intan Technologies, Los Angeles, CA, USA) connected to the Open Ephys acquisition system via an ultra-thin SPI interface cable (Intan Technologies). The raw signal was acquired at 30 kHz sampling rate, bandpass filtered (0.1-7500 Hz) and stored for offline analysis. During the experiment, simultaneous electrophysiological and video recordings were acquired with the Open Ephys GUI software.

2.4 | Data analysis for in vivo electrophysiology

For data analysis purposes, three zones were defined in the OF: The center zone, consisting of a 25 cm diameter circle in the center (25% of total OF area), a transition zone between the center and the periphery, consisting of a 37.5 cm diameter circle but excluding the center zone (31% of total OF area), and the periphery, consisting of everything not included in the center or transition zones (44% of total OF area). For behavioral analysis, time, distance traveled, average speed and number of visits into the center zone were analyzed. For electrophysiological analysis, LFP power and coherence were calculated in the OF center and periphery. The Bonsai software[31] was used to extract the location of the mouse in each video frame. The set of coordinates were imported to MATLAB, where location and speed were calculated. LFPs were analyzed in custom-written MATLAB scripts. The signal was filtered between 0.7 and 400 Hz using a zero-phase distortion FIR filter and down sampled to 1 kHz. To exclude potential locomotion influences in the LFP recordings, only periods of exploration with a speed >7 cm/s were analyzed. To this end, electrophysiological traces in which the animals were moving with a speed of 7-40 cm/s in the habituation condition and periphery of the open field were extracted and concatenated into one continuous trace. The power spectrum was calculated using the *pwelch* function in MATLAB with 1 second windows and 0.8 second overlap. To obtain coherence values, the imaginary part of the cross power spectral density was computed and normalized to the square root of the product of the auto power spectral densities, using the same window and overlap. The imaginary coherence is sensitive only to time-lagged signals, thus avoiding contamination of the coherence values by volume conduction.[32,33] The following frequency band ranges were used: Delta, 2-6 Hz; Theta: 6-12 Hz; Beta: 15-30 Hz; Gamma: 35-70 Hz. To obtain an individual value of power for each animal, the power within a given frequency band was summed. To obtain the average coherence value per brain region within a given frequency band, the maximum coherence value of one brain region with each of the other four regions was calculated, and these four values were then averaged. Finally, a grand average was calculated for each genotype. To obtain the power and coherence correlations as a function of time spent in the center, the linear correlation coefficient (*fitlm* function, MATLAB) was calculated using the power and coherence values computed for each mouse and included mice from all genotypes. The Granger causality was calculated using the Multivariate Granger Causality Toolbox,[32,34] based on the same unfiltered LFP traces used for coherence and power calculations. The order of the vector autoregressive (VAR) model to be fitted was calculated using the Akaike information criterion. Individual Granger causality values per animal were obtained by calculating the average values within a frequency band. To obtain the Granger causality correlations as a function of location in the OF, the Granger causality was computed as above for each mouse for the whole OF session using a sliding window of 1 second of the raw unfiltered

LFP traces with 50% overlap, resulting in a 0.5 second time resolution. Location and speed in the OF were extracted by matching the timestamps of the OF with those of the Granger causality spectrogram. The individual values were binned (1 cm bins) and normalized to the average Granger values in the periphery (>20 cm from center), and the linear correlations per genotype were computed. To control for speed of the mouse during exploration of the OF, partial correlations (*partialcorr* function, MATLAB) were computed using speed and interaction between speed and location as control variables. The slopes of the adjusted linear fits of each genotype were used as the modulation index with the distance from the OF (Figure 4G). To statistically compared the linear fits between genotypes, analysis of covariance (*aoctool* function, MATLAB) was performed using the adjusted Granger values.

2.5 | Generation and validation of *Nlgn2* conditional KO (cKO) mice

Nlgn2 cKO mice were generated by insertion of loxP sites into the flanking regions of *Nlgn2* exon 2 (which contains the start codon, see Figure 5 for details). LoxP sites were inserted using homologous recombination[35] based on the *Nlgn2*-containing BAC clone RPCIB731L16422Q[36] (ImaGenes GmbH, Berlin, Germany). Targeted embryonic stem (ES) cells were generated using the wildtype C57BL/6N ES cell clone JM8A3[37] (EUCOMM). Correct targeting of ES cell clones was confirmed by PCR analysis using a set of primers that generated five PCR products. Two of these products (5′ long and 5′ short) were additionally digested with BamHI to confirm correct integration of the 5′ loxP site (which is associated with a BamHI site). Conditional KO mice were generated by blastocyst injection of targeted ES cell clone 8E02, and the Neo cassette was removed by crossing the mice with a Flp recombinase driver line. *Nlgn2* cKO mice were backcrossed to a C57BL/6JRj background for at least six generations before experimental use.

To confirm that *Nlgn2* cKO show normal expression of Nlgn2 in the absence of Cre, Nlgn2 protein levels were determined in tissue homogenate from WT/WT, Fl/WT and Fl/Fl mice using standard immunoblotting procedures as previously described,[38] using a mouse monoclonal primary antibody against Nlgn2 (clone 5E6, Synaptic Systems, Göttingen, Germany, diluted 1:500) and a goat anti-mouse IRDye800-labeled secondary antibody (Rockland Immunochemicals, Pottstown, PA, USA, diluted 1:2500). Equal protein loading was confirmed using a Memcode reversible protein stain (Thermo Fisher Scientific, Waltham, MA, USA) as previously described.[38] To confirm efficacy of Nlgn2 deletion and emergence of the anxiety phenotype following deletion of Nlgn2 in adulthood, *Nlgn2* cKO (Fl/Fl) mice were crossed with a Tamoxifen-inducible Cre driver (ROSA26_CreERT2) generated in the laboratory of Tyler Jacks[39] and obtained from the Jackson Laboratory (Bar Harbor, ME, USA). Tamoxifen dissolved in corn oil (Sigma Aldrich, St. Louis, MO, USA) was injected intraperitoneally for 5 consecutive days, 2x per day at 100 mg/kg. Six weeks after administration of Tamoxifen, mice were tested in the open field exactly as previously described[17,20] and subsequently sacrificed for analysis of Nlgn2 protein levels as above.

2.6 | Generation of AAV-GFP and AAV-GFP/Cre viruses

To locally delete Nlgn2 using local expression of Cre recombinase, AAV5 vectors were generated using the AAV-GFP and AAV-GFP/Cre plasmids generously provided by Fred Gage[40] (Addgene plasmids 49055 and 49056, Watertown, MA, USA) in combination with the pDP5rs packaging system (PlasmidFactory, Bielefeld, Germany) as previously described.[20] Briefly, plasmids were transfected into HEK cells using polyethylenimine transfection, and virus particles were harvested 48-72 hours later. To this end, HEK cells were lysed for 30 minutes at 37°C in 20 mM Tris, pH 8.0, containing 150 mM NaCl, 0.5% sodium deoxycholate and benzonase, followed by incubation in 1 M NaCl at 56°C for 30 minutes. Lysates were stored at −80°C overnight, thawed, and purified on a 15%/25%/40%/54% iodixanol gradient by ultracentrifugation (90 minutes at 370 000*g*). The 40% fraction was collected, diluted in PBS containing 1 mM $MgCl_2$ and 2.5 mM KCl, and concentrated using an Amicon 100K MWCO filter (Merck Millipore, Burlington, MA, USA). To confirm efficacy of Nlgn2 deletion by AAV5-GFP/Cre, dissociated hippocampal cultures from *Nlgn2* cKO mice were infected with AAV5-GFP or AAV5-GFP/Cre 24 hours after plating. After 14 days, cultures were harvested and Nlgn2 protein levels were determined by immunoblotting.

2.7 | Stereotaxic injection of AAV-GFP and AAV-GFP/Cre viruses

Mice were anesthetized with Avertin (loading dose 20 mL/kg, maintenance dose 2 mL/kg i.p.). Anesthetized mice were placed in a digital stereotaxic frame, and an incision in the midline of the scalp was made to expose the skull. Bregma and lambda were aligned to a plane level ±50 µm. 0.8 µL of virus was injected bilaterally into the BLA (−0.8 mm AP, ±3.2 mm ML and −5.2 mm DV) or the vHPC (−2.3 mm AP, ±3.2 mm ML and −4.2 mm DV) using a Nanoject II Microinjector (Drummond, Broomall, PA, USA) and a Micro pump controller (WPI, Sarasota, FL, USA). Mice were alternately assigned to receive AAV-GFP or AAV-GFP/Cre

injections based on order of birth. Immediately after the surgery, mice received subcutaneous analgesic (Carprofen 10 mg/kg). 24 hours after the surgery, mice received Metamizol in the drinking water (1.6 mg/mL). After surgery, mice were housed in pairs and were allowed to recover for 6 weeks before behavioral analysis.

2.8 | OF behavior following virus injections

Open field behavior following stereotaxic virus injection was performed as previously described.[17,20] One week before and six weeks after surgery, mice were placed into a square open field chamber made of white plastic (50 × 50 cm) with a light intensity of 20 lux, and they were permitted to explore the chamber for 10 minutes. Performance was recorded using an overhead camera system and scored automatically using the Viewer software (Biobserve, St. Augustin, Germany). Between each mouse, the arena was cleaned thoroughly with 70% ethanol followed by water to eliminate any odors left by the previous mouse. Three behavioral zones were analyzed: The center zone, consisting of a 25 × 25 cm square in the center (25% of total OF area), a transition zone between the center and the periphery, consisting of a 37.5 × 37.5 cm square but excluding the center zone (31% of total OF area), and the periphery, consisting of everything not included in the center or transition zones (44% of total OF area). For each zone, time, distance traveled, average speed and number of visits into the zone were analyzed. Additionally, immobility behavior was analyzed by extracting speed and location information in the Bonsai software, with immobility defined as the animal moving with a speed <2 cm/s. Data from the post-injection OF test were normalized to the pre-injection OF test (post-injection OF/pre-injection OF × 100) as previously described[20] in order to minimize the effects of between-animal variability and reduce animal numbers. One animal that was highly anxious even prior to the surgery (defined as <20 seconds in the center of the OF in the pre-injection OF) was excluded from the experiment.

2.9 | Verification of AAV injection sites, viral spread and Nlgn2 protein levels

Following OF testing, mice were perfused transcardially with saline and 4% paraformaldehyde (PFA), and free-floating sections (40 µm thickness) from BLA or vHPC were prepared as previously described.[20] Photomicrographs of endogenous GFP fluorescence at the injection site were acquired using a SP8 confocal microscope (Leica, Wetzlar, Germany). Tiled 20X images covering the brain slice were obtained using a 20X immersion objective and then stitched using the Leica SP8 software stitching function (LAS X Stitching). For each mouse, GFP fluorescence intensity was measured using the ImageJ software from the brain section that contains the injection site, as well as from one anterior and one posterior section to the injection site. Fluorescence intensity above threshold from all mice per group was combined to generate an overview over the extent of maximum viral spread (Figure S9).

For quantification of Nlgn2 levels following virus injection, which requires an immunohistochemical protocol that is not compatible with measurement of endogenous GFP fluorescence, a separate set of mice was injected with AAV-GFP or AAV-GFP/Cre into BLA as described above. Six weeks after surgery, mice were sacrificed and brains were processed for Nlgn2 immunohistochemistry using methanol-fixed fresh frozen brain sections as previously described.[20] The following primary antibodies were used: guinea pig anti-Nlgn2 (Synaptic Systems, Göttingen, Germany, diluted 1:500) and rabbit anti-GFP (Synaptic Systems, diluted 1:500). The following secondary antibodies were used: Goat anti-mouse and goat anti-rabbit labeled with Alexa Fluor Dyes A555 and A488, respectively (Thermo Fisher Scientific, Waltham, MA, USA, diluted 1:600). Photomicrographs of Nlgn2 and GFP immunohistochemistry at the injection site were acquired using a Leica SP8 confocal microscope with a 63x oil immersion objective. Imaging parameters were kept constant across both conditions, and all images were acquired within one session. Image analysis was conducted using the ImageJ software. Binary images were created manually using a threshold value of 3x image background intensity, then segmented with the "analyze particles" function to quantify Nlgn2 puncta per image.

2.10 | Statistical analysis

Data were analyzed statistically using MATLAB or GraphPad Prism. Prior to analysis, LFP data from mistargeted electrodes were removed, leaving the following final sample numbers (out of originally 17 mice per group): WT vHPC, 14; KO vHPC, 12, WT mPFC, 13; KO mPFC, 13; WT BLA, 11; KO BLA, 9; WT BNST, 6; KO BNST, 9; WT CeM, 6; WT CeM, 6. For AAV-GFP/Cre injections, behavior data from mice with mistargeting of the viral expression were removed, leaving the following final sample numbers: WT BLA, 8 out of 10 total; KO BLA, 9 out of 11 total; WT vHPC, 10 out of 10 total; KO vHPC; 12 out of 12 total.

For all data sets, normal distribution was first assessed using the Shapiro Wilk normality test, and outliers were subsequently removed using the standard deviation method for parametric data sets (outliers defined as values >2x standard deviation from the mean) and the interquartile range method for non-parametric data sets (outliers defined as values 1.5x interquartile range from the upper or lower quartile).

Behavior data were analyzed using unpaired, two-tailed Student's t-tests or Mann-Whitney tests for parametric and non-parametric data sets, respectively. In vivo electrophysiological data for LFP power and coherence were analyzed using two-way ANOVA with repeated measures, with location (habituation context, OF periphery, OF center) and genotype (WT, *Nlgn2* KO) as the two factors. Data from four *Nlgn2* KO mice had to be excluded from the ANOVA analysis because they had not entered the OF center at all, and accordingly, no LFP recordings in the OF center were available for analysis. Posthoc analysis was performed using the Fisher's LSD test with subsequent adjustment for multiple comparisons using false discovery rate (FDR) correction across all ANOVA analyses in the experiment. For correlations between LFP power or coherence and behavior, Pearson's or Spearman's correlation coefficients were calculated for parametric and non-parametric data sets, respectively. Data for Granger directionality were analyzed using unpaired, two-tailed Student's t-tests or Mann-Whitney tests for parametric and non-parametric data sets, respectively, and *P* values were adjusted for multiple comparisons using FDR correction.

3 | RESULTS

3.1 | Deletion of Nlgn2 alters LFP power throughout the defensive network

In order to assess how deletion of Nlgn2 alters information processing throughout the network mediating defensive behaviors, we recorded LFPs, which mainly reflect the combined synaptic activity of local and distant inputs,[41] simultaneously in the mPFC, vHPC, BLA, CeM and BNST of male WT and *Nlgn2* KO mice. To this end, electrodes were implanted into all five brain regions (see Figure S1 for electrode placements), and one week later, mice were tethered to the acquisition system and LFPs were recorded both during a brief habituation phase in the home cage and during exploration of a circular OF arena (Figure 1A-C). Under these conditions, *Nlgn2* KO mice showed a pronounced avoidance of the anxiogenic center of the OF as previously reported,[17,19,20] including a reduction in time spent, distance traveled, and entries made into the center (Figure 1D,E, red bars compared to WT, black bars, see also Figure S2A,B). LFPs were analyzed in the habituation phase and during exploration of the OF periphery and the OF center, which presumably represent increasingly aversive contexts. In all conditions, LFP analysis was restricted to periods of active exploration (defined as locomotor speed >7 cm/s) to eliminate variability due to differences in locomotion. Due to the technical challenge of targeting five brain regions simultaneously, some electrodes were mistargeted and had to be removed from the analysis, resulting in the final sample numbers reported in the figures.

Spectral analysis of LFPs in WT vs. *Nlgn2* KO mice revealed distinctive patterns of oscillatory activity in the delta (2-6 Hz), theta (6-12 Hz), beta (15-30 Hz) and gamma (35-70 Hz) frequency ranges (Figure 1F). Comparison of LFP power in these frequency ranges across the three contexts (habituation context (=HC), OF periphery and OF center; Figure 1G-R for vHPC, mPFC, and BLA, Figure S2C,D for CeM and BNST) showed that exposure to the OF resulted in a robust modulation in activity in the vHPC, mPFC and BLA, which have been proposed to form a tripartite circuit that plays a central role in mediating defensive behaviors.[4,21,24,25] Consistent with these reports, mice displayed a significant increase in LFP power in the theta frequency range in the OF compared to the habituation context in both the vHPC-mPFC-BLA circuit and in the CeM (Figures 1J-L and S2C; two-way ANOVA with factors genotype and context (repeated measures); $^{\#}$ denotes significant main effect of context; see Table S1 for detailed ANOVA values). Moreover, gamma power in the vHPC-mPFC-BLA circuit was significantly reduced in the OF (Figure 1P-R), with no significant modulation of beta power (Figure 1M-O) and a minor reduction in delta power only in the BLA (Figure 1G-I). No significant differences were observed in the BNST and few in the CeM (Figure S2C,D), although this may result in part from an increased challenge in correctly targeting these small structures and hence from lower sample numbers.

Direct comparison of LFP power in the OF in WT and *Nlgn2* KO mice revealed a striking increase in power in the vHPC of *Nlgn2* KO compared to WT mice that spanned all frequency ranges (Figure 1G,J,M,P; $^{\%}$ denotes significant main effect of genotype; see also Table S1). It is important to note that the robust increase in theta power in vHPC of *Nlgn2* KO mice was not detected by electrodes in nearby regions such as the BLA and CeM, highlighting both the specificity of the recordings and the low contamination by volume conduction. Moreover, more modest differences were observed in beta power in the BLA and the CeM (Figures 1O and S2C, consistent with our previous report[20]), in gamma power in the mPFC (Figure 1Q) and in delta power in the CeM (Figure S2C). Interestingly, the differences in power were largely present even in the habituation context, indicating either that the *Nlgn2* KO mice were already more anxious than WT mice during habituation (eg due to handling during attachment of the head stage and tethering to the acquisition system) or that these differences were not immediately related to the aversive context. A differential modulation with context was observed only in gamma power in the mPFC, where *Nlgn2* KO mice displayed a reduction in LFP power during habituation, which was not further reduced upon transition to the OF (Figure 1Q; § denotes a significant context x genotype interaction). Together, these data indicate that deletion of Nlgn2

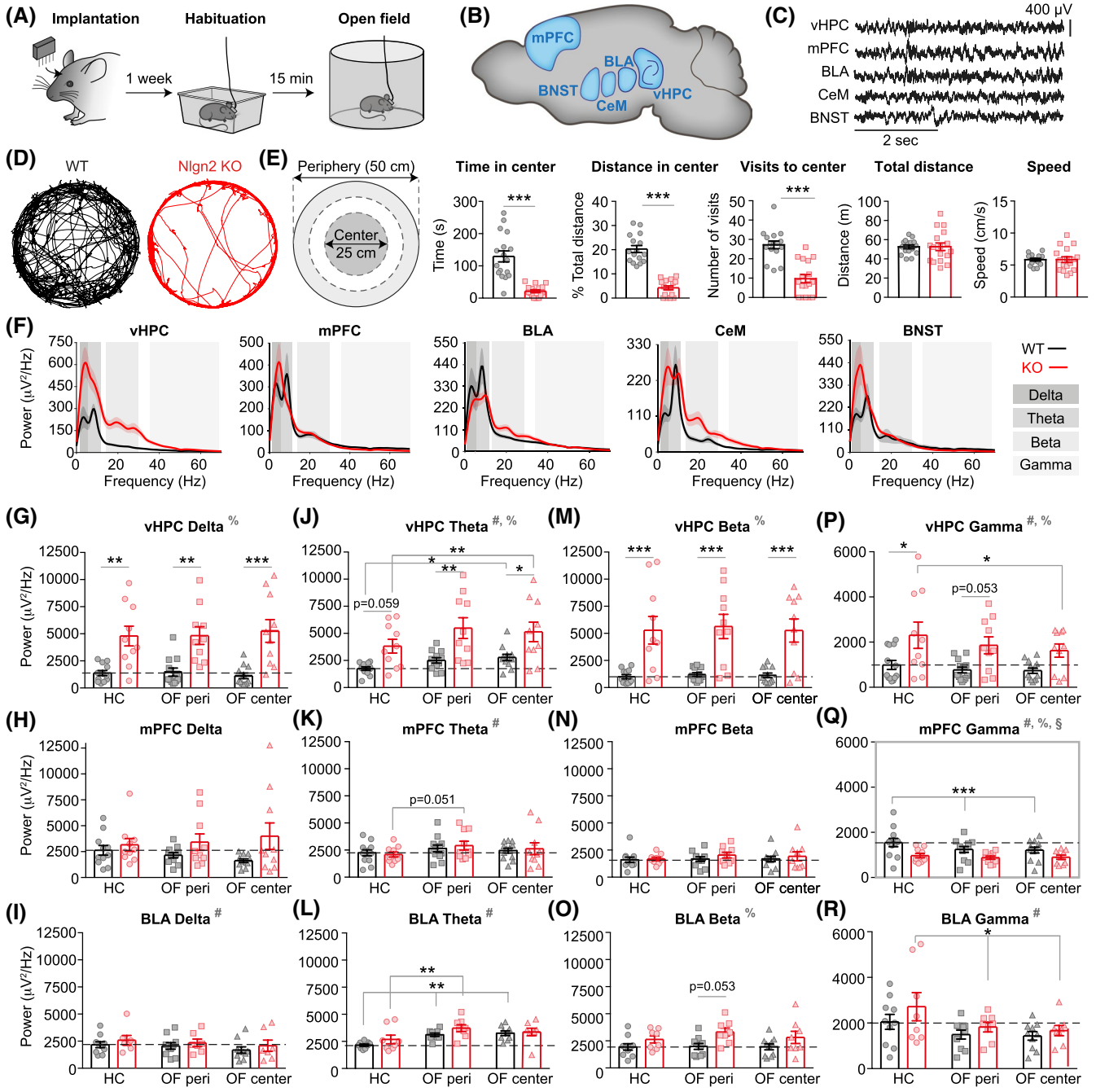

FIGURE 1 Deletion of Nlgn2 alters neuronal activity throughout the circuit mediating defensive behaviors. A, Schematic of the experimental procedure for the in vivo electrophysiological recordings. B, Schematic of the brain regions recorded with a circuit approach (adapted from[3]). C, Example of LFP traces recorded during exploration of the OF. D, Representative tracks of the OF exploration. E, Schematic representation of the periphery (light grey) and center (dark grey) zones analyzed; and quantification of time spent in the anxiogenic center of the OF; distance travel in the center of the OF; visits to the center of the OF; total distance travelled in the OF and average speed during exploration of the OF. F, LFP power spectrum of the different brain regions recorded during OF exploration. G-I, Average delta power of WT and *Nlgn2* KO animals in the vHPC (G), mPFC (H), and BLA (I). J-L, Average theta power of WT and *Nlgn2* KO animals in the vHPC (J), mPFC (K), and BLA (L). M-O, Average beta power of WT and *Nlgn2* KO animals in the vHPC (M), mPFC (N), and BLA (O). P-R Average gamma power of WT and *Nlgn2* KO animals in the vHPC (P), mPFC (Q), and BLA (R). HC = Habituation context, OF peri = OF periphery. Two-way ANOVA for context (repeated factor) and genotype: #significant main effect of context; %significant main effect of genotype; §significant context x genotype interaction. A grey border around a graph highlights a significant context × genotype interaction. Posthoc Fisher's LSD test with FDR correction for multiple comparisons: Significant pairwise context comparisons are indicated by asterisks above the grey lines connecting the bars. Significant pairwise genotype comparisons are indicated by asterisks immediately above the red KO bar. *$P < .05$, **$P < .01$, ***$P < .001$. n for each group indicated on the bar graphs. Black bars = WT, red bars = Nlgn2 KO. Error bars represent *SEM*. See Table S1 for detailed statistics and precise animal numbers

results in a pronounced overactivation of the vHPC and more subtle alterations in activity in the mPFC-BLA-CeM network that are present across multiple contexts.

3.2 | Deletion of Nlgn2 alters synchrony within the avoidance circuitry during OF exploration

Information processing in the brain relies critically on efficient communication between brain regions within a network, and indeed, disruptions in the functional connectivity between brain regions are thought to play a role in several psychiatric disorders,[42-44] including anxiety disorders.[45,46] Such functional connectivity can be reflected in the synchronization of oscillatory activity across regions.[42-44] To determine whether the excessive avoidance behavior observed in *Nlgn2* KO mice was accompanied by alterations in neural synchrony, we measured the imaginary coherence between brain regions both in the habituation context and during OF exploration and calculated the coherence for each pair of brain regions (Figures 2, S3 and Table S1). The imaginary coherence is sensitive only to time-lagged signals (see Methods) and thus mostly reduces contamination from signals that occur simultaneously in other brain regions. Since in general, similar patterns of coherence changes were observed across pairs of brain regions for each frequency range, we also generated an average coherence score for each brain region for ease of comparison (Figure S4 and Table S1).

Comparison of average LFP coherence across the three contexts showed that exposure to the OF resulted in a significant modulation of coherence in all assessed frequency ranges, with WT mice showing a modest increase in average mPFC theta coherence with increasing aversiveness of the context and a robust decrease in average coherence in the beta, gamma and delta frequency ranges in the OF periphery compared to the habituation context (Figure S4, two-way ANOVA with factors genotype and context (repeated measures); $^{\#}$ denotes significant main effect of context, * denotes significant post-hoc comparison; see Table S1 for detailed ANOVA values). Analysis of individual pairs of brain regions in WT mice indicated that these decreases were driven primarily by significant reductions in coherence in the pairs vHPC-mPFC (delta, gamma Figure 2D,M), vHPC-BLA (delta, beta gamma; Figure 2E,K,N), and mPFC-BLA (gamma; Figure 2O). In *Nlgn2* KO mice, despite the fact that LFP power in the theta frequency range was increased both compared to WT mice in the vHPC (Figure 1J) and upon transition from the habituation context to the OF (Figure 1J-L), average theta coherence was consistently lower in *Nlgn2* KO mice compared to WT mice in the habituation context and OF periphery (Figure S4, $^{\%}$ denotes significant main effect of genotype, * denotes significant post-hoc comparison). Nevertheless, a significant increase in theta coherence upon transition to the aversive OF center was observed in the vHPC-mPFC and vHPC-BLA connections (Figure 2G,H), possibly reflecting the transfer anxiety-related context information. Concomitant with these alterations in theta coherence, *Nlgn2* KO mice displayed a striking increase in beta and gamma coherence within the vHPC-mPFC-BLA network compared to WT mice, which was specifically observed in the OF but not in the habituation context (Figure 2J-O, § denotes a significant context x genotype interaction, * denotes a significant post-hoc comparison). It should be noted that accurate calculation of the LFP coherence values in the *Nlgn2* KO mice is challenging due to the short time spent by these mice in the OF center, which may bias toward higher coherence values. Indeed, restricting the analysis of data from WT mice in the OF center to the first 20 seconds, corresponding to the average time window for the *Nlgn2* KOs, resulted in an apparent increase in LFP coherence in the beta and gamma, but not delta and theta frequencies (Figure S5 and Table S1). As a consequence, changes in beta and gamma coherence in *Nlgn2* KO mice from the OF periphery to the OF center should be interpreted with caution. Nevertheless, regardless of analysis window chosen for the WTs, *Nlgn2* KO mice displayed significant and pronounced increases in vHPC-BLA beta, vHPC-BLA gamma and mPFC-BLA gamma coherence compared to WT mice that were specific to the OF (Figure 2K,N,O). Together, these data indicate that *Nlgn2* KO mice display an overall reduction in average theta coherence that is accompanied by an exaggerated increase upon transition to the anxiogenic OF center, as well as an increase in beta and gamma coherence in specific connections in the vHPC-mPFC-BLA circuitry.

3.3 | Altered LFP coherence correlates with avoidance behavior in *Nlgn2* KO mice

To determine whether either LFP power or average coherence in the OF center may represent a physiological correlate of the excessive center avoidance behavior observed in *Nlgn2* KO mice, we calculated linear correlations between each of these measurements and time spent in the center of the OF (Figure 3A). Surprisingly, we found that LFP power overall correlated poorly with OF center time, the only exception being a significant correlation with delta and beta power in the vHPC (summarized in Figure 3B, * denotes a significant correlation; see Figure S6 for individual graphs and Table S1 for statistical analysis). In contrast, LFP coherence emerged as the primary correlate of avoidance behavior, with OF center time significantly correlated with average beta and gamma coherence of the vHPC, mPFC and BLA, as well as with average delta coherence of the vHPC, mPFC and

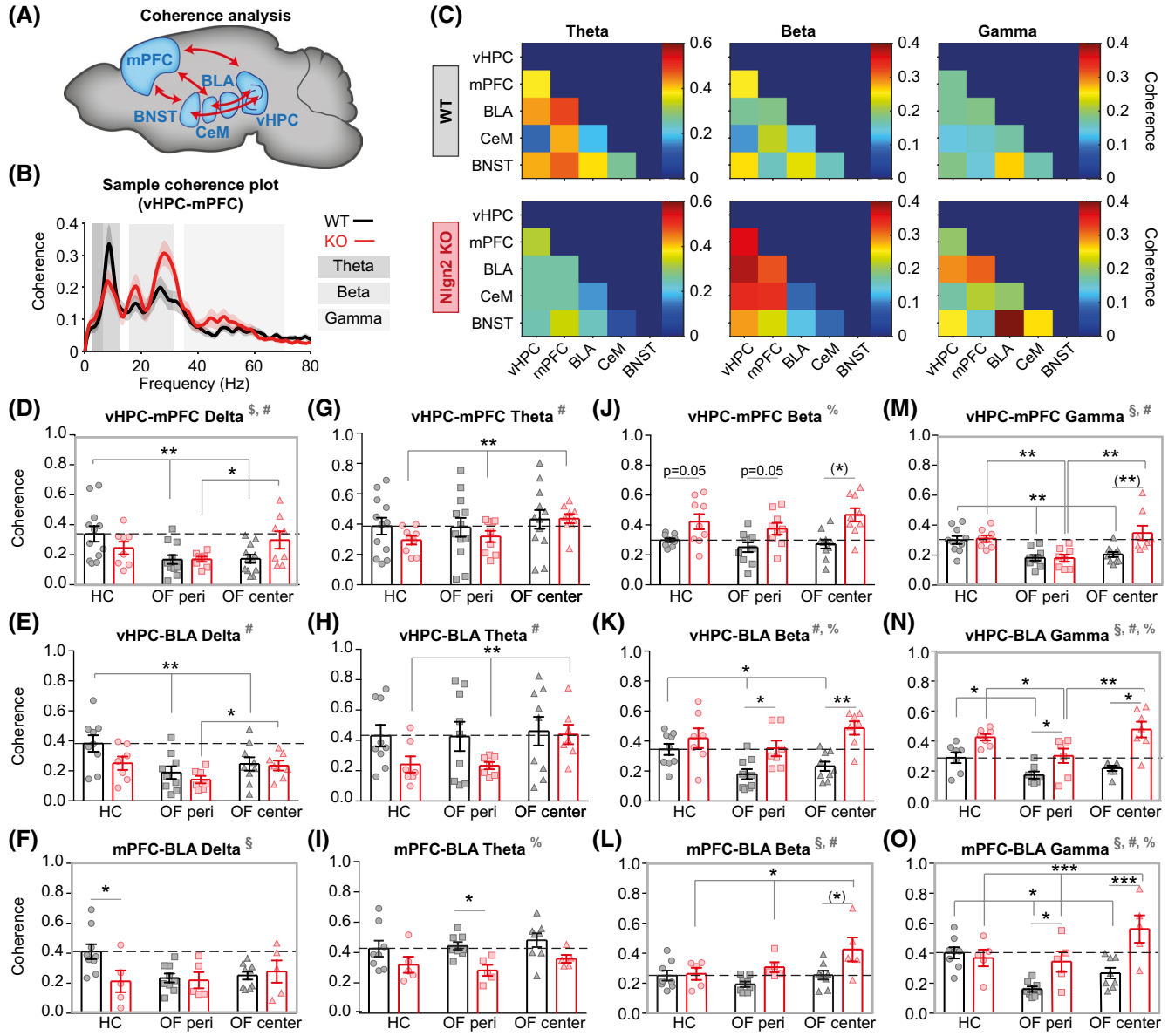

FIGURE 2 Deletion of Nlgn2 alters LFP coherence in the circuit mediating defensive behaviors. A, Schematic of the pairs of brain regions used for the coherence analysis. B, Example of average imaginary coherence for pairs of brain regions simultaneously recorded during exploration of the open field. C, Average coherence values for all the pairs of brain regions for WT (top) and *Nlgn2* KO mice (bottom). D-F Average delta coherence of WT and *Nlgn2* KO animals in the vHPC (D), mPFC (E) and BLA (F). G-I Average theta coherence of WT and *Nlgn2* KO animals in the vHPC (G), mPFC (H) and BLA (I). J-L Average beta coherence of WT and *Nlgn2* KO animals in the vHPC (J), mPFC (K) and BLA (L). M-O Average gamma coherence of WT and *Nlgn2* KO animals in the vHPC (M), mPFC (N) and BLA (O). HC = Habituation context, OF peri = OF periphery. Two-way ANOVA for context (repeated factor) and genotype: $^{\#}$significant main effect of context; $^{\%}$significant main effect of genotype; $^{\$}$significant context × genotype interaction. A grey border around a graph highlights a significant context × genotype interaction. Posthoc Fisher's LSD test with FDR correction for multiple comparisons: Significant pairwise context comparisons are indicated by asterisks above the grey lines connecting the bars. Significant pairwise genotype comparisons are indicated by asterisks immediately above the red KO bar. $^{*}P < .05$, $^{**}P < .01$, $^{***}P < .001$, $^{(*)}$ denotes WT-KO comparisons in the OF center that are no longer significant following time window adjustment in WT mice (see text and Figure S5 for details). Error bars represent *SEM*. Black bars = WT, red bars = *Nlgn2* KO. See Table S1 for detailed statistics and precise animal numbers

CeM (summarized in Figure 3C, * denotes a significant correlation; see Figure S7 for individual graphs and Table S1 for statistical analysis). Analysis of the correlation of OF center time with LFP coherence between individual pairs of brain regions revealed that OF center time in *Nlgn2* KO mice (but interestingly not in WT mice) was most prominently correlated with vHPC-mPFC coherence in the delta, beta and gamma frequency ranges (Figure 3D, Pearson's r correlation

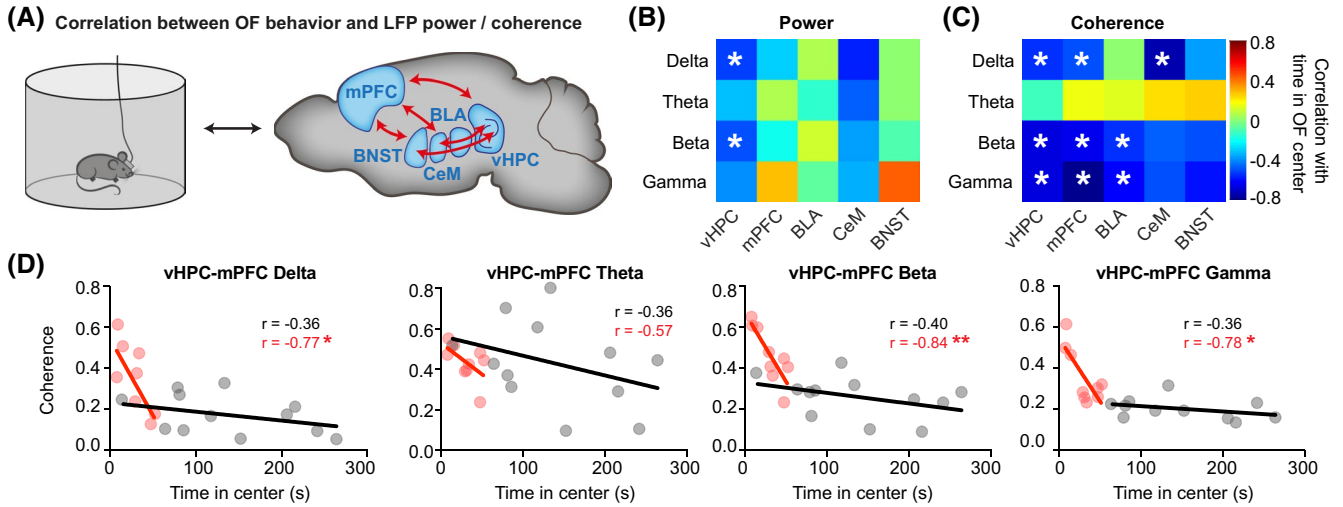

FIGURE 3 LFP coherence, but not LFP power, strongly correlates with avoidance behavior across brain regions. A, Schematic of the correlation analysis. B, Summary correlation matrix showing the correlation coefficients between anxiety behavior and average LFP power of each brain region in the delta, theta, beta, and gamma frequency ranges. See Figure S6 and Table S1 for detailed statistics and precise animal numbers. C, Summary correlation matrix showing the correlation coefficients between anxiety behavior and average coherence of each brain region in the delta, theta, beta, and gamma frequency ranges. See Figure S7 and Table S1 for detailed statistics and precise animal numbers. The asterisks indicate a significant correlation between anxiety behavior and LFP power or coherence. D, Correlations of OF center time with coherence between the vHPC and the mPFC in different frequency bands. Pearson correlation coefficient for WT (black) and *Nlgn2* KO (red) indicated on each graph. $^{*}P < .05$, $^{**}P < .01$. n = 6-13 mice per genotype

coefficient for WT and *Nlgn2* KO indicated on the graph; * denotes a significant correlation), with no other significant pairwise correlations observed in *Nlgn2* KO mice. These findings indicate that LFP coherence is a stronger correlate of avoidance behavior than LFP power, and that the coherence between the vHPC and the mPFC plays a particularly pronounced role in the excessive avoidance behavior observed in *Nlgn2* KO mice.

3.4 | Deletion of Nlgn2 alters directed functional connectivity in the theta and beta frequency ranges during OF exploration

To further investigate this altered synchrony, and in particular to assess alterations in the directionality of connectivity which could not be determined from the previous analysis, we performed a Granger causality analysis as a measure of directed functional connectivity in the frequency domain[32,34] (Figure 4A). In WT mice, high Granger causality values were observed in the vHPC→mPFC, vHPC→BLA and BLA→mPFC directions, specifically in the theta frequency range (Figure 4B, quantified in Figure 4C). These findings are consistent with previous reports indicating that the vHPC is causally involved in generating theta oscillations in the mPFC and BLA which contribute to the context-dependent regulation of anxiety-related behaviors.[4,21-25] In contrast, this leading role of vHPC theta oscillations was completely absent in *Nlgn2* KO mice. Instead, robust increases in Granger causality values in the beta frequency range were observed, particularly in the mPFC→vHPC, vHPC→BLA, vHPC→CeM, and CeM→vHPC directions (Figure 4D), indicating that in the absence of Nlgn2, the vHPC and mPFC may exert their influence on the BLA and the CeM most strongly in the beta frequency range. Fewer differences between WT and *Nlgn2* KO mice were observed in the delta and gamma frequency ranges (Figure 4E,F), indicating that Granger causality in these frequency bands may be less relevant for the *Nlgn2* KO phenotype. Importantly, the differences between WT and *Nlgn2* KO mice were largely not present in the habituation context (Figure S8), and they are therefore likely to specifically reflect the anxiogenic nature of the OF.

3.5 | Deletion of Nlgn2 disrupts dynamic modulation of theta and beta directionality with spatial location in the OF

The above analyses were performed using Granger causality values that were averaged across all spatial locations in the OF and across the entire time period of the behavioral test. Accordingly, dynamic changes in directionality that occurred during exploration of individual spatial locations within the OF, most notably the more aversive center vs. the less aversive periphery, would not have been identified in these analyses. To overcome this limitation and assess whether any of the directionality measures were differentially modulated between WT and *Nlgn2* KO mice in

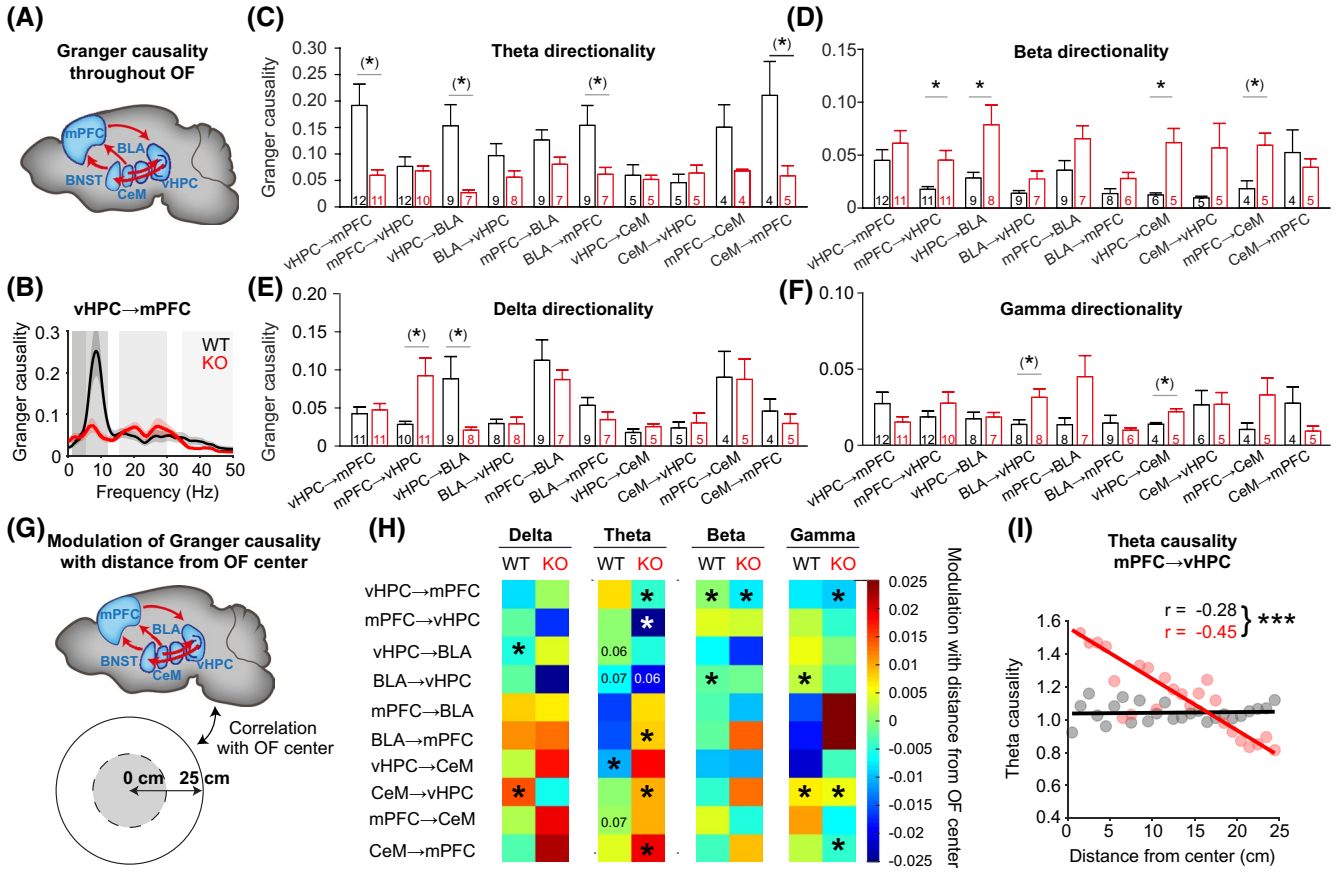

FIGURE 4 Nlgn2 deletion alters vHPC-mPFC-BLA directionality. A, Schematic of the Granger directionality analysis. B, Example of average Granger causality for pairs of brain regions simultaneously recorded during exploration of the OF. C-F, Average Granger causality in the theta (C), beta (D), delta (E) and gamma (F) frequency ranges. G, Schematic of the correlation analysis between Granger causality and location in the OF. H, Summary modulation matrix showing the slopes of the adjusted linear fit between Granger causality in the delta, theta, beta and gamma ranges and location in the OF. The asterisks indicate a significant correlation between Granger causality and OF location. I, Correlation of changes in theta Granger causality with location in the OF in the mPFC → vHPC direction. $*P < .05$, $***P < .001$, $^{(*)}$ denotes WT-KO comparisons that are significant by Student's t-test or Mann-Whitney test, but not following FDR correction. n for each group indicated on the bar graphs. Error bars represent *SEM*

different spatial locations, we calculated the correlation between each directionality measure and the distance from the aversive center of the OF separately for both genotypes (Figure 4G). To prevent any confounding effect of locomotion, we computed partial correlations which control for both the speed and the interaction between speed and location (see Methods). In WT mice, Granger causality in the theta frequency range was significantly modulated with OF location in the vHPC→CeM direction (asterisk in Figure 4H, theta column), with trends towards significant modulation in the vHPC→BLA, BLA→vHPC and mPFC→CeM directions. In *Nlgn2* KO mice, the modulation of theta directionality within the vHPC-mPFC-BLA circuit was strongly exaggerated (asterisks in Figure 4H, theta column), with a striking increase in directionality during approach to the OF center particularly in the mPFC→vHPC direction that was significantly different from WT (Figure 4I). In contrast, theta directionality between the mPFC and the CeM decreased significantly during OF center approach. Unlike theta directionality, Granger causality in the beta frequency range was less strongly modulated with OF location, with significant but weak correlations only in the vHPC→mPFC and BLA→vHPC directions in WT mice and in vHPC→mPFC direction in *Nlgn2* KO (Figure 4H, beta column). In the delta and gamma frequency bands, only modest albeit in some cases significant correlations were observed, indicating again that Granger causality in these frequency bands may be less relevant for the *Nlgn2* KO phenotype.

Together, these data indicate that Nlgn2 deletion disrupts the appropriate modulation of Granger causality with OF location most prominently in the theta and beta frequency ranges. In the theta frequency range, it results in an overall aberrant decrease in Granger directionality during OF exploration, with exaggerated increases in the tripartite vHPC-mPFC-BLA circuit as the animals move toward the center of the OF. In the beta frequency range, Nlgn2 deletion induces excessive Granger directionality during OF exploration, which fails to be regulated dynamically during approach to the center of the OF.

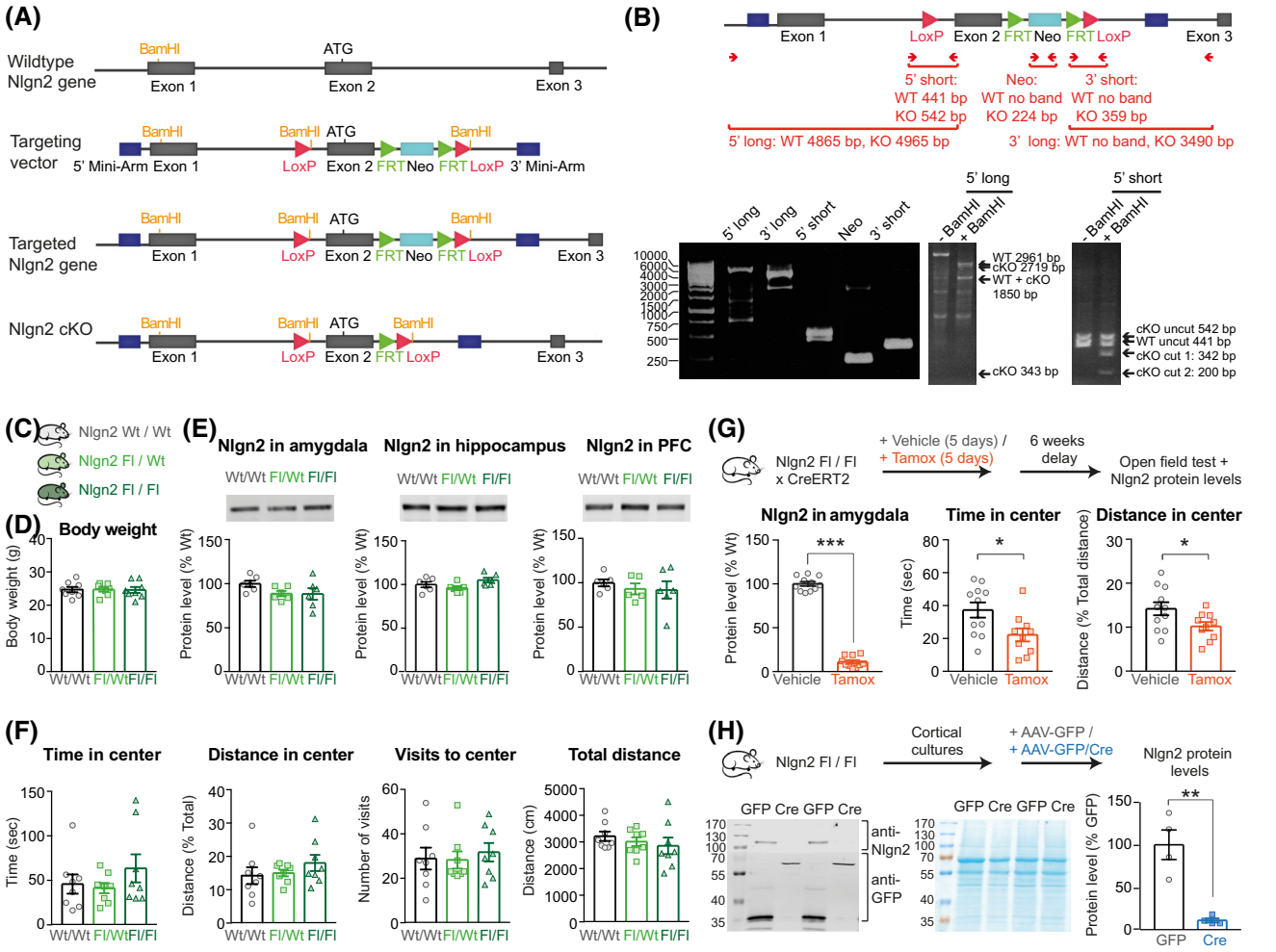

FIGURE 5 Generation and validation of *Nlgn2* cKO mice. A, Schematic representation of the strategy used to generate *Nlgn2* cKO mice (see methods section for details). B, PCR screening of ES cell clone 8E02. Schematic in the top panel represents the five PCR products generated using the depicted primer sets. Expected band sizes are marked with arrows. All products correspond to the bands expected from a correctly targeted ES cell clone. C, *Nlgn2* cKO mice homozygous (Fl/Fl) or heterozygous (Fl/Wt) for the floxed allele were compared to WT littermates (Wt/Wt) in several measures relating to anxiety behavior. D, No significant differences were observed between Wt/Wt, Fl/Wt and Fl/Fl mice in body weight. One-way ANOVA: $F_{2,21} < 1$. E, No significant differences were observed in Nlgn2 protein levels in the amygdala (one-way ANOVA: $F_{2,15} = 1.94$, $P = .178$), hippocampus (one-way ANOVA: $F_{2,15} = 2.81$, $P = .091$) or prefrontal cortex (one-way ANOVA: $F_{2,14} = 0.378$, $P = .692$). F, No significant differences were observed in any behavioral parameter in the open field test (one-way ANOVA: $F_{2,21} < 1$ for all behavioral comparisons). G, Following Tamoxifen administration in *Nlgn2* Fl/Fl × CreERT2 mice, Nlgn2 protein levels in the amygdala were strongly reduced, and anxiety behaviors were increased, confirming that deletion of Nlgn2 in adulthood has an anxiogenic effect. H, In dissociated hippocampal cultures, Nlgn2 levels were significantly reduced following infection with AAV-GFP/Cre compared to infection with AAV-GFP, confirming the AAV-GFP/Cre viruses were effective in deleting Nlgn2. All bars represent mean + *SEM*, $*P < .05$, $**P < .01$

3.6 | vHPC and BLA contribute to distinct aspects of defensive behavior in *Nlgn2* KO mice

To begin to isolate the contribution of individual components of the circuitry mediating defensive behaviors to the *Nlgn2* KO phenotype, we generated *Nlgn2* conditional KO (cKO) mice (Figure 5) and deleted Nlgn2 locally using stereotaxic injection of AAV vectors expressing Cre recombinase (AAV5-GFP/Cre) or a GFP control (AAV5-GFP) (Figures 6 and S9). Given that it had been previously shown that local deletion of Nlgn2 in the mPFC is anxiolytic,[47] possibly reflecting the function of the mPFC in top-down control over the BLA, we focused our analysis on the BLA and the vHPC. To this end, we recorded OF behavior before and six weeks after the stereotaxic injection of AAV-GFP/Cre into the vHPC or the BLA of adult male homozygous cKO mice based on previous reports[47] (Figure 6A,B). These experiments showed that deletion of Nlgn2 from both the vHPC and the BLA resulted in a phenotype that recapitulated aspects of the defensive behavior in the constitutive *Nlgn2* KO mice (Figure 1D,E and Refs17,20), but with different patterns. Specifically,

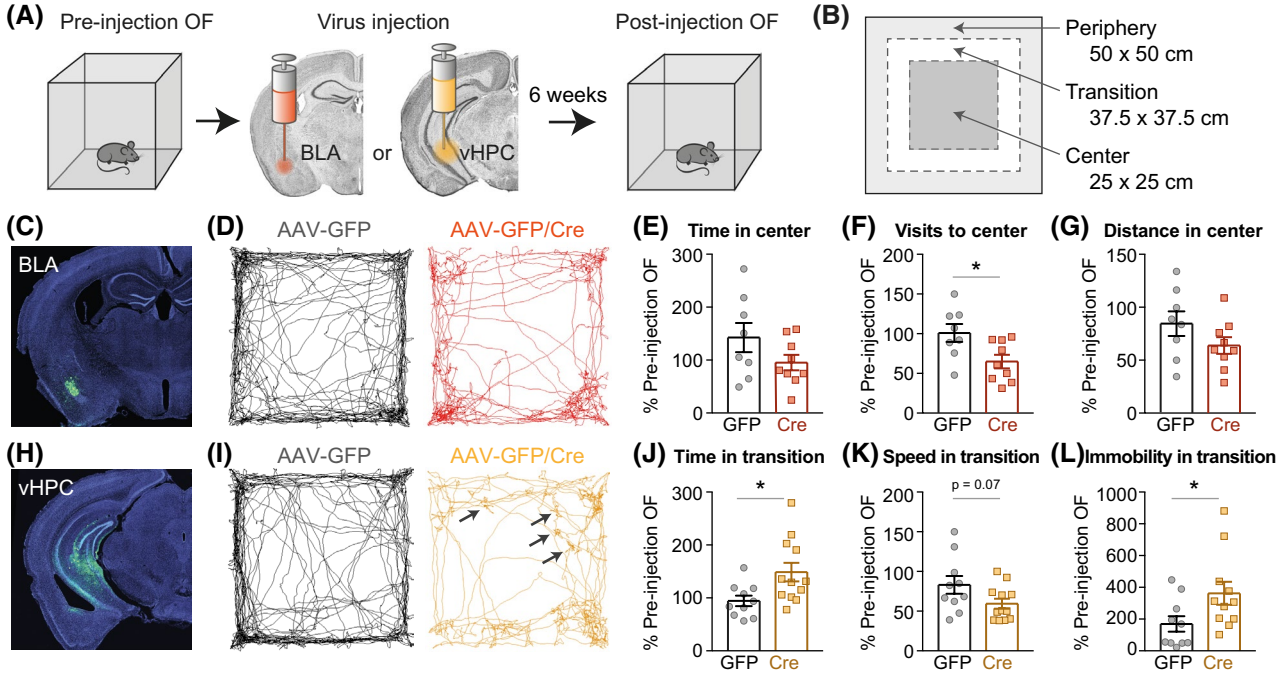

FIGURE 6 vHPC and BLA encode distinct aspects of the *Nlgn2* KO center avoidance phenotype. A, Experimental design for stereotaxic injection of AAV-GFP or AAV-GFP/Cre into BLA or vHPC. B, Schematic representation of the periphery (light grey), transition (white) and center (dark grey) zones analyzed. C, Example photomicrograph representing the virus injection site in the BLA. D, Representative tracks of OF exploration following virus injection in the BLA. E-G, Time in center of OF (E), visits to center of OF (F) and distance travelled in the center of OF (G) following virus injection in the BLA. H, Example photomicrograph representing the virus injection site in the vHPC. I, Representative tracks of OF exploration following virus injection in the vHPC. J-L, Time in the transition zone (J), speed in the transition zone (K), and time spent immobile in the transition zone (L) following virus injection in the vHPC. Two-tailed Student's t-test: $*P < .05$. n for each group indicated on the bar graphs. Error bars represent *SEM*. See Table 1 for full set of parameters and detailed statistics

deletion of Nlgn2 from the BLA resulted in a reduction in the number of visits to the center, likely reflecting anxiety-induced changes in exploratory behavior[17] (Figure 6C-G and Table 1). In contrast, deletion of Nlgn2 from the vHPC did not affect the behavior of the mice in the center of the OF (Figure 6H-L and Table 1). Instead, it resulted in an increase in immobility specifically upon transition from the safe periphery to the anxiogenic center as reflected by an increase in the time spent in the transition zone (Figure 6J), a trend toward a reduction in the speed of movement in this zone (Figure 6K), and a pronounced increase in the time spent immobile (Figure 6L). Visual inspection of the tracks confirmed that AAV-GFP/Cre-injected animals showed noticeable segments of immobility, indicated by black arrows on the representative tracks, which based on comparison with video data appeared to reflect freezing upon entry into the anxiogenic transition zone. These data indicate that the two brain regions both contribute to alterations in defensive behavior resulting from Nlgn2 deletion but may encode separate aspects of defensive behaviors, with the BLA being critical for reductions in exploration under aversive conditions and the vHPC for threat-induced freezing behaviors.

4 | DISCUSSION

In the present study we show that excessive avoidance behavior in mice lacking in inhibitory synapse-associated protein Nlgn2 is associated with alterations in functional connectivity between key brain regions in the network mediating defensive behaviors. In particular, pronounced increases in LFP power in the vHPC of *Nlgn2* KO mice were accompanied by an abnormal theta frequency synchrony modulation particularly in the tripartite vHPC-mPFC-BLA circuit, as well as by a widespread increase in beta and gamma frequency synchrony. Moreover, altered coherence between brain regions, but not LFP power within individual brain regions, correlated strongly with avoidance behaviors. Local deletion of Nlgn2 from the BLA and vHPC revealed distinct roles of Nlgn2 in these brain regions in encoding defensive behaviors, with the BLA and vHPC mediating reduced exploratory activity and immobility in transition to the center, respectively. Together, these observations support two key conclusions: (1) The consequences of Nlgn2 deletion for avoidance behaviors are not primarily mediated by local effects within a given brain region, such as local alterations in LFP power, but likely result from abnormalities in the communication between key regions in the

TABLE 1 Consequences of local *Nlgn2* deletion from BLA or vHPC on behavior in the OF

	GFP				Cre				*P*
	Mean	**±**	**SEM**	**n**	**Mean**	**±**	**SEM**	**n**	**value**
BLA									
Center									
Time	142.5	±	27.6	8	95.2	±	14.7	9	.139
Distance	84.5	±	11.7	8	63.8	±	7.8	9	.154
Visits	**100.9**	±	**11.3**	**8**	**64.9**	±	**8.5**	**9**	**.021**
Speed	74.5	±	11.9	8	74.6	±	8.1	9	.996
Immobility	318.5	±	173.9	6	504.1	±	233.8	8	.852
Transition									
Time	123.7	±	6.4	8	129.3	±	8.0	8	.597
Distance	78.8	±	8.1	8	69.5	±	4.7	9	.327
Visits	97.7	±	5.7	8	95.2	±	8.6	9	.817
Speed	66.0	±	9.0	8	53.9	±	2.6	9	.195
Immobility	250.6	±	51.3	7	253.2	±	21.4	8	.963
Periphery									
Time	90.6	±	3.1	8	94.2	±	1.3	9	.276
Distance	71.9	±	9.4	8	62.5	±	3.9	9	.351
Visits	88.7	±	3.6	8	106.5	±	10.3	9	.470
Speed	78.1	±	8.7	8	66.4	±	4.2	9	.229
Immobility	140.4	±	18.3	7	176.0	±	16.3	8	.168
vHPC									
Center									
Time	81.2	±	18.4	9	91.7	±	12.7	12	.578
Distance	67.3	±	10.3	9	61.3	±	6.7	12	.557
Visits	103.2	±	28.8	9	92.7	±	17.2	11	.839
Speed	88.5	±	8.1	10	74.2	±	9.0	12	.260
Immobility	224.8	±	123.3	9	546.7	±	246.7	12	.306
Transition									
Time	**94.5**	±	**9.9**	**10**	**136.9**	±	**17.5**	**11**	**.026**
Distance	72.0	±	6.8	10	81.0	±	6.8	12	.363
Visits	89.9	±	5.9	10	91.1	±	7.3	12	.905
Speed	83.1	±	11.1	10	59.4	±	6.2	12	.067
Immobility	**169.0**	±	**48.6**	**10**	**448.1**	±	**108.3**	**12**	**.021**
Periphery									
Time	102.3	±	3.5	10	94.0	±	3.9	12	.136
Distance	74.6	±	7.8	10	64.1	±	6.8	12	.325
Visits	93.2	±	5.3	10	94.8	±	7.1	12	.860
Speed	72.9	±	6.8	10	68.8	±	7.1	12	.688
Immobility	151.0	±	11.8	9	164.9	±	21.5	11	.600

Bold values highlight statistically significant differences between mice injected with AAV-GFP and AAV-GFP/Cre.

anxiety network. (2) Loss of Nlgn2 results in both exaggerated activation of known defensive circuits, particularly an increase in theta coherence between the vHPC, mPFC and BLA in aversive contexts, and fundamentally distinct mechanisms, ie a threat-associated increase in beta and gamma coherence not observed in WT mice. Our findings have important implications for developing and evaluating potential anxiolytic strategies in animal models of pathological anxiety.

The observation that the exaggerated avoidance behavior in *Nlgn2* KO mice most reliably correlates with LFP coherence between brain regions rather than LFP power within any given region highlights the importance of assessing and understanding alterations in long-range connectivity in both patients and in animal models of pathological anxiety. *Nlgn2* KO mice displayed a dramatic increase in LFP power across frequency bands in the vHPC, as well as more modest alterations in beta power in the BLA and CeM (consistent with our previous findings[20]) and in gamma power in the mPFC. However, despite the fact that all of these brain regions have been prominently implicated in the circuits mediating defensive behaviors,[1,4,5,21-29,48] the alterations in LFP power were not specific to the OF center, and only weak correlations were observed with OF center time as a measure of avoidance behavior. In contrast, LFP coherence within the vHPC-mPFC-BLA network was prominently modulated by aversiveness of the context and correlated significantly with OF center time. These findings indicate that correcting these alterations in LFP coherence may be an important aim for any therapeutic strategy for pathological anxiety related to alterations in Nlgn2 function (and potentially in synaptic inhibition in general).

Prominent among the alterations in LFP coherence in *Nlgn2* KO was a reduced theta synchrony in the OF periphery and an exaggerated increase upon approach of the aversive center. This observation is consistent with previous findings showing that the exploration of an aversive environment is accompanied by an increase in theta frequency synchrony within vHPC-mPFC-BLA circuit in anxious but not in non-anxious WT mice.[21,22,24,25] It has been proposed that theta synchrony between the vHPC and the mPFC encodes certain aspects of the context relevant to anxiety, while theta synchrony between the mPFC and the BLA may contribute to the discrimination between safe and aversive contexts.[4,24,25,30] Interestingly, we did not observe significant anxiety-related increases in theta coherence in our WT mice, indicating that they may correspond to non-anxious WT mice as previously defined,[24] possibly due to reasons of strain background or procedural details. Importantly, however, *Nlgn2* KO mice showed a significant increase in vHPC-mPFC and vHPC-BLA synchrony upon approaching the aversive OF center, supporting the notion that the prominent avoidance phenotype observed in the *Nlgn2* KO mice results at least in part from an exaggerated activation of normal anxiety-related theta transmission.

In addition to theta oscillations, gamma power and theta-gamma coupling in the mPFC-BLA circuit have been linked to fear behaviors, and it has been proposed that gamma activity in this circuit may signal safety and lead to suppression of defensive behaviors.[49] Consistent with this notion, we observed a significant reduction in gamma power in the mPFC and BLA as animals move from the habituation context to the OF, and gamma power in the mPFC of *Nlgn2* KO mice was reduced compared to WTs across contexts. Similarly, gamma synchrony decreased markedly in WT mice upon exposure to the OF, particularly in the mPFC-BLA circuit. Surprisingly, however, a pronounced increase in gamma synchrony was observed in *Nlgn2* KO mice, particularly in the aversive OF center, indicating that, unlike in WT mice, mPFC-BLA gamma coherence is unlikely to contribute to the identification of safe contexts in *Nlgn2* KO mice.

Intriguingly, *Nlgn2* KO mice additionally displayed an abnormally high coherence in the beta frequency range, and increased beta coherence was associated with avoidance of the aversive OF center in *Nlgn2* KO but not in WT mice. These findings support the hypothesis that, in addition to excessive activation of the circuits underlying normal, adaptive anxiety, a fundamentally distinct mechanism contributes to the pathological anxiety phenotype displayed by the *Nlgn2* KO mice. This is particularly intriguing in light of the fact that relatively little is known about the role of beta oscillations in general, and to our knowledge, the role of beta frequency synchrony in defensive networks has never been explored in animal models. Previous studies have identified a role for beta power in decision-making[50,51] and context representation,[52] as well as an increase in beta synchrony between the thalamus and the mPFC during working memory.[53] We recently showed that beta power is increased in the CeM of *Nlgn2* KO mouse under anxiogenic conditions, and that this increase is normalized by a manipulation that also normalized the avoidance behavior.[20] Here, we expand these findings to indicate that beta synchrony throughout the network mediating defensive behaviors may represent a neural signature of pathological anxiety processing in *Nlgn2* KO mice. In support of this hypothesis, it was recently shown that amygdala-hippocampal beta coherence as well as the theta/beta ratio strongly correlates with anxiety traits in human subjects.[54,55] An important implication that arises from our findings is that information about the networks underlying physiological, adaptive anxiety cannot necessarily be generalized to those involved in pathological anxiety states, and that conclusions drawn from studies on WT mice will need to be verified in appropriate animal models of pathological anxiety.

An interesting remaining question is whether the LFP alterations observed here in *Nlgn2* KO mice in the OF also contribute to their phenotype in other anxiety-related tests. We have previously shown that *Nlgn2* KO mice display prominent avoidance of the open arm in an elevated plus maze (EPM) and of the light compartment in a light/dark box.[17,20] Unfortunately, we were unable to record LFPs from *Nlgn2* KO mice in the EPM due to their tendency to occasionally fall off the open arms, a phenotype that was incompatible with the tethering of the mice to the acquisition system. Similarly, the tethering precluded recordings in the closed compartment of the light/dark box. Wireless recording systems would be necessary to overcome these limitations in future experiments.

The molecular basis for the observed alterations in LFP power or coherence resulting from Nlgn2 deletion remain to be elucidated. Nlgn2 is a key organizer protein at inhibitory synapses throughout the forebrain,[8,10,11,15-18] and synaptic inhibition is well known to play a central role in the generation of local oscillatory activity.[56-61] In particular, deletion of Nlgn2 is thought to most prominently affect perisomatic inhibitory synapses, likely those originating from parvalbumin (PV)-positive interneurons.[10,15-17] These synapses have been particularly implicated in the generation of oscillations in the gamma frequency range,[57,61,62] and consistent with this notion, we previously showed that deletion of the Nlgn2-related Neuroligin-4 (Nlgn4) protein, which shares many properties with Nlgn2 at least in mice, results in pronounced alterations in gamma oscillatory activity in hippocampal slices.[38] However, recent evidence indicates that PV-positive interneurons also contribute to the generation of theta and potentially beta frequency oscillations,[56,60,63,64] indicating that deletion of Nlgn2 may directly affect the power or coherence of these frequency ranges. Further analysis of the mechanistic link between Nlgn2 deletion and the generation of theta and beta oscillations will be essential toward understanding how alterations in synaptic inhibition contribute to anxiety disorders.

An equally important open question regards the contribution of Nlgn2 in different brain regions to the observed physiological and behavioral phenotypes. Our data indicate that disinhibition in the vHPC may contribute to the increased avoidance behavior in *Nlgn2* KO mice, resulting in dramatic increases in vHPC LFP power as well as in alterations in vHPC-mediated functional connectivity during OF exploration. In accordance with this notion, local deletion of Nlgn2 from the vHPC resulted in a pronounced increase in immobility in the transition zone from the safe periphery to the anxiogenic center of the OF, possibly at the point of decision regarding entry into the center vs. retreat into the periphery. Nevertheless, this manipulation does not recapitulate many of the consequences of constitutive Nlgn2 deletion, making it unlikely for the vHPC to be the sole origin of the behavioral phenotype (although other factors, such as limited virus spread or developmental effects in the constitutive KO, may also contribute to the differences). Indeed, local deletion of Nlgn2 in the BLA resulted in a significant reduction in visits to the center of the OF, consistent with the notion that Nlgn2 in the BLA may contribute specifically to the threat-induced reductions in exploratory behavior that we previously reported in *Nlgn2* KO mice.[17] Moreover, a previous study showed that deletion of Nlgn2 in the mPFC resulted in a behavioral phenotype opposite to that observed in the constitutive *Nlgn2* KO, with a reduction in avoidance behaviors in the OF and EPM,[47] possibly reflecting the top-down regulatory role of the mPFC over the anxiogenic output of the amygdala. It is also possible that loss of Nlgn2 in brain regions not investigated here may contribute to the behavioral phenotype of the constitutive *Nlgn2* KO mice. For example, local manipulations of Nlgn2 in the lateral septum[65] and nucleus accumbens[66] were recently shown to affect stress responsiveness and defensive behaviors.

Altogether, our findings indicate that deletion of Nlgn2 may have widespread consequences throughout the circuitry mediating defensive behaviors, and that the prominent avoidance phenotype induced by deletion of Nlgn2 results from a combination of known and novel mechanisms compared to those in WT mice. *Nlgn2* KO mice thus represent a highly relevant model to study the molecular and circuitry mechanisms by which alterations in synaptic inhibition may result in pathological anxiety behavior.

ACKNOWLEDGEMENTS

The authors are grateful to Dr Nils Brose for his continuous support of their research in the Department of Molecular Neurobiology, which is funded by the Deutsche Forschungsgesellschaft (CNMPB and SFB1190/P10) and the Bundesministerium für Bildung und Forschung (ERA-NET Neuron Synpathy). DK-B. was funded by a NARSAD Young Investigator Grant (Brain & Behavior Research foundation). OB was supported by a PhD fellowship from the Minerva Foundation. CPC was a student of the Neurasmus Master program and was supported by an Erasmus Mundus scholarship (European Commission). VM was supported by an IMPRS stipend (Max Planck Society). NB was supported by a traineeship from the ERASMUS+ placement program (European Commission). The authors are grateful to Nikolas Karalis for sharing his code to calculate Granger causality and to Fritz Benseler, the AGCT Lab, the MPIEM animal facility and the Feinmechanik for excellent technical support.

CONFLICT OF INTEREST

The authors declare no competing financial interests.

AUTHOR CONTRIBUTIONS

DK-B., HC-S. and OB conceived the study. HC-S. designed, performed and analyzed in vivo electrophysiology experiments. DK-B. and OB designed experiments involving local deletion of Nlgn2 in *Nlgn2* cKO mice. OB and HA performed stereotaxic injection of AAV constructs into *Nlgn2* cKO as well as subsequent behavioral experiments and data analysis. DK-B. and SW generated the *Nlgn2* cKO mouse line. SW, NB and HA performed molecular and behavioral validation of the *Nlgn2* cKO mouse line. SW generated AAV particles for injection. CPC assisted with stereotaxic surgeries and behavior experiments. VM assisted with in vivo electrophysiology and behavior experiments. DK-B. provided supervision for all experiments. DK-B., HC-S. and OB wrote the paper, and all authors edited and approved the final manuscript.

ORCID

Dilja Krueger-Burg https://orcid.org/0000-0001-5597-6287

REFERENCES

1. Tovote P, Fadok JP, Luthi A. Neuronal circuits for fear and anxiety. *Nat Rev Neurosci*. 2015;16:317-331.
2. Craske MG, Stein MB. Anxiety. *Lancet*. 2016;388:3048-3059.
3. Calhoon GG, Tye KM. Resolving the neural circuits of anxiety. *Nat Neurosci*. 2015;18:1394-1404.
4. Adhikari A. Distributed circuits underlying anxiety. *Front Behav Neurosci*. 2014;8:112.
5. Babaev O, Piletti Chatain C, Krueger-Burg D. Inhibition in the amygdala anxiety circuitry. *Exp Mol Med*. 2018;50:18.
6. Mohler H. The GABA system in anxiety and depression and its therapeutic potential. *Neuropharmacology*. 2012;62:42-53.
7. Engin E, Benham RS, Rudolph U. An emerging circuit pharmacology of GABAA receptors. *Trends Pharmacol Sci*. 2018;39:710-732.
8. Krueger-Burg D, Papadopoulos T, Brose N. Organizers of inhibitory synapses come of age. *Curr Opin Neurobiol*. 2017;45:66-77.
9. Varoqueaux F, Jamain S, Brose N. Neuroligin 2 is exclusively localized to inhibitory synapses. *Eur J Cell Biol*. 2004;83:449-456.
10. Poulopoulos A, Aramuni G, Meyer G, et al. Neuroligin 2 drives postsynaptic assembly at perisomatic inhibitory synapses through gephyrin and collybistin. *Neuron*. 2009;63:628-642.
11. Ali H, Marth L, Krueger-Burg D. Neuroligin-2 as a central organizer of inhibitory synapses in health and disease. *Sci Signal*. 2020;13:eabd8379.
12. Sun C, Cheng M-C, Qin R, et al. Identification and functional characterization of rare mutations of the neuroligin-2 gene (NLGN2) associated with schizophrenia. *Hum Mol Genet*. 2011;20:3042-3051.
13. Parente DJ, Garriga C, Baskin B, et al. Neuroligin 2 nonsense variant associated with anxiety, autism, intellectual disability, hyperphagia, and obesity. *Am J Med Genet A*. 2017;173:213-216.
14. Shillington A, Lamy M, Vawter-Lee M, et al. Case report: is catatonia a clinical feature of the natural progression of NLGN2-related neurodevelopmental disorder? *J Autism Dev Disord*. 2021;51:371-376.
15. Gibson JR, Huber KM, Sudhof TC. Neuroligin-2 deletion selectively decreases inhibitory synaptic transmission originating from fast-spiking but not from somatostatin-positive interneurons. *J Neurosci*. 2009;29:13883-13897.
16. Jedlicka P, Hoon M, Papadopoulos T, et al. Increased dentate gyrus excitability in neuroligin-2-deficient mice in vivo. *Cereb Cortex*. 2011;21:357-367.
17. Babaev O, Botta P, Meyer E, et al. Neuroligin 2 deletion alters inhibitory synapse function and anxiety-associated neuronal activation in the amygdala. *Neuropharmacology*. 2016;100:56-65.
18. Varoqueaux F, Aramuni G, Rawson RL, et al. Neuroligins determine synapse maturation and function. *Neuron*. 2006;51:741-754.
19. Blundell J, Tabuchi K, Bolliger MF, et al. Increased anxiety-like behavior in mice lacking the inhibitory synapse cell adhesion molecule neuroligin 2. *Genes Brain Behav*. 2009;8:114-126.
20. Babaev O, Cruces-Solis H, Piletti Chatain C, et al. IgSF9b regulates anxiety behaviors through effects on centromedial amygdala inhibitory synapses. *Nat Commun*. 2018;9:5400.
21. Adhikari A, Topiwala MA, Gordon JA. Synchronized activity between the ventral hippocampus and the medial prefrontal cortex during anxiety. *Neuron*. 2010;65:257-269.
22. Adhikari A, Topiwala MA, Gordon JA. Single units in the medial prefrontal cortex with anxiety-related firing patterns are preferentially influenced by ventral hippocampal activity. *Neuron*. 2011;71:898-910.
23. Felix-Ortiz A, Beyeler A, Seo C, et al. BLA to vHPC inputs modulate anxiety-related behaviors. *Neuron*. 2013;79:658-664.
24. Likhtik E, Stujenske JM, Topiwala MA, Harris AZ, Gordon JA. Prefrontal entrainment of amygdala activity signals safety in learned fear and innate anxiety. *Nat Neurosci*. 2014;17:106-113.
25. Padilla-Coreano N, Bolkan SS, Pierce GM, et al. Direct ventral hippocampal-prefrontal input is required for anxiety-related neural activity and behavior. *Neuron*. 2016;89:857-866.
26. Tye KM, Prakash R, Kim S-Y, et al. Amygdala circuitry mediating reversible and bidirectional control of anxiety. *Nature*. 2011;471:358-362.
27. Lee SC, Amir A, Haufler D, Pare D. Differential recruitment of competing valence-related amygdala networks during anxiety. *Neuron*. 2017;96:81-88 e85.
28. Kim S-Y, Adhikari A, Lee SY, et al. Diverging neural pathways assemble a behavioural state from separable features in anxiety. *Nature*. 2013;496:219.
29. Gründemann J, Bitterman Y, Lu T, et al. Amygdala ensembles encode behavioral states. *Science*. 2019;364:eaav8736.
30. Padilla-Coreano N, Canetta S, Mikofsky RM, et al. Hippocampal-prefrontal theta transmission regulates avoidance behavior. *Neuron*. 2019;104:601-610.e4.
31. Lopes G, Bonacchi N, Frazão J, et al. Bonsai: an event-based framework for processing and controlling data streams. *Front Neuroinform*. 2015;9:7.
32. Karalis N, Dejean C, Chaudun F, et al. 4-Hz oscillations synchronize prefrontal-amygdala circuits during fear behavior. *Nat Neurosci*. 2016;19:605-612.
33. Nolte G, Bai OU, Wheaton L, et al. Identifying true brain interaction from EEG data using the imaginary part of coherency. *Clin Neurophysiol*. 2004;115:2292-2307.
34. Barnett L, Seth AK. The MVGC multivariate Granger causality toolbox: a new approach to Granger-causal inference. *J Neurosci Methods*. 2014;223:50-68.
35. Liu P, Jenkins NA, Copeland NG. A highly efficient recombineering-based method for generating conditional knockout mutations. *Genome Res*. 2003;13:476-484.
36. Osoegawa K, Tateno M, Woon PY, et al. Bacterial artificial chromosome libraries for mouse sequencing and functional analysis. *Genome Res*. 2000;10:116-128.
37. Pettitt SJ, Liang QI, Rairdan XY, et al. Agouti C57BL/6N embryonic stem cells for mouse genetic resources. *Nat Methods*. 2009;6:493.
38. Hammer M, Krueger-Burg D, Tuffy L, et al. Perturbed hippocampal synaptic inhibition and γ-oscillations in a neuroligin-4 knockout mouse model of autism. *Cell Rep*. 2015;13:1-8.
39. Ventura A, Kirsch DG, McLaughlin ME, et al. Restoration of p53 function leads to tumour regression in vivo. *Nature*. 2007;445:661-665.
40. Kaspar BK, Vissel B, Bengoechea T, et al. Adeno-associated virus effectively mediates conditional gene modification in the brain. *Proc Natl Acad Sci USA*. 2002;99:2320.
41. Buzsáki G, Anastassiou CA, Koch C. The origin of extracellular fields and currents—EEG, ECoG, LFP and spikes. *Nat Rev Neurosci*. 2012;13:407.
42. Harris AZ, Gordon JA. Long-range neural synchrony in behavior. *Ann Rev Neurosci*. 2015;38:171-194.
43. Mathalon DH, Sohal VS. Neural oscillations and synchrony in brain dysfunction and neuropsychiatric disorders: it's about time. *JAMA Psychiatry*. 2015;72:840-844.

44. Uhlhaas PJ, Singer W. Neural synchrony in brain disorders: relevance for cognitive dysfunctions and pathophysiology. *Neuron*. 2006;52:155-168.
45. Xu J, Van Dam NT, Feng C, et al. Anxious brain networks: A coordinate-based activation likelihood estimation meta-analysis of resting-state functional connectivity studies in anxiety. *Neurosci Biobehav Rev*. 2019;96:21-30.
46. Sylvester CM, Corbetta M, Raichle ME, et al. Functional network dysfunction in anxiety and anxiety disorders. *Trends Neurosci*. 2012;35:527-535.
47. Liang J, Xu W, Hsu Y-T, et al. Conditional neuroligin-2 knockout in adult medial prefrontal cortex links chronic changes in synaptic inhibition to cognitive impairments. *Mol Psychiatry*. 2015;20:850-859.
48. Lebow MA, Chen A. Overshadowed by the amygdala: the bed nucleus of the stria terminalis emerges as key to psychiatric disorders. *Mol Psychiatry*. 2016;21:450-463.
49. Stujenske JM, Likhtik E, Topiwala MA, Gordon JA. Fear and safety engage competing patterns of theta-gamma coupling in the basolateral amygdala. *Neuron*. 2014;83:919-933.
50. Haegens S, Nacher V, Hernandez A, et al. Beta oscillations in the monkey sensorimotor network reflect somatosensory decision making. *Proc Natl Acad Sci USA*. 2011;108:10708.
51. Leventhal D, Gage G, Schmidt R, et al. Basal ganglia beta oscillations accompany cue utilization. *Neuron*. 2012;73:523-536.
52. Berke JD, Hetrick V, Breck J, Greene RW. Transient 23–30 Hz oscillations in mouse hippocampus during exploration of novel environments. *Hippocampus*. 2008;18:519-529.
53. Parnaudeau S, O'Neill P-K, Bolkan S, et al. Inhibition of mediodorsal thalamus disrupts thalamofrontal connectivity and cognition. *Neuron*. 2013;77:1151-1162.
54. Kirkby LA, Luongo FJ, Lee MB, et al. An amygdala-hippocampus subnetwork that encodes variation in human mood. *Cell*. 2018;175:1688-1700.e1614.
55. Putman P, van Peer J, Maimari I, van der Werff S. EEG theta/beta ratio in relation to fear-modulated response-inhibition, attentional control, and affective traits. *Biol Psychol*. 2010;83:73-78.
56. Chen G, Zhang Y, Li X, et al. Distinct inhibitory circuits orchestrate cortical beta and gamma band oscillations. *Neuron*. 2017;96:1403-1418.e1406.
57. Mann EO, Paulsen O. Role of GABAergic inhibition in hippocampal network oscillations. *Trends Neurosci*. 2007;30:343-349.
58. Korotkova T, Ponomarenko A, Monaghan CK, et al. Reconciling the different faces of hippocampal theta: the role of theta oscillations in cognitive, emotional and innate behaviors. *Neurosci Biobehav Rev*. 2018;85:65-80.
59. Bocchio M, Nabavi S, Capogna M. Synaptic plasticity, engrams, and network oscillations in amygdala circuits for storage and retrieval of emotional memories. *Neuron*. 2017;94:731-743.
60. Stark E, Eichler R, Roux L, et al. Inhibition-induced theta resonance in cortical circuits. *Neuron*. 2013;80:1263-1276.
61. Sohal VS, Zhang F, Yizhar O, Deisseroth K. Parvalbumin neurons and gamma rhythms enhance cortical circuit performance. *Nature*. 2009;459:698-702.
62. Bartos M, Vida I, Jonas P. Synaptic mechanisms of synchronized gamma oscillations in inhibitory interneuron networks. *Nat Rev Neurosci*. 2007;8:45-56.
63. Wulff P, Ponomarenko AA, Bartos M, et al. Hippocampal theta rhythm and its coupling with gamma oscillations require fast inhibition onto parvalbumin-positive interneurons. *Proc Natl Acad Sci USA*. 2009;106:3561.
64. Amilhon B, Huh C, Manseau F, et al. Parvalbumin interneurons of hippocampus tune population activity at theta frequency. *Neuron*. 2015;86:1277-1289.
65. Troyano-Rodriguez E, Wirsig-Wiechmann CR, Ahmad M. Neuroligin-2 determines inhibitory synaptic transmission in the lateral septum to optimize stress-induced neuronal activation and avoidance behavior. *Biol Psychiatry*. 2019;85:1046-1055.
66. Heshmati M, Aleyasin H, Menard C, et al. Cell-type-specific role for nucleus accumbens neuroligin-2 in depression and stress susceptibility. *Proc Natl Acad Sci USA*. 2018;115:1111-1116.

SUPPORTING INFORMATION

Additional Supporting Information may be found online in the Supporting Information section.

How to cite this article: Cruces-Solis H, Babaev O, Ali H, et al. Altered theta and beta oscillatory synchrony in a genetic mouse model of pathological anxiety. *The FASEB Journal*. 2021;35:e21585. https://doi.org/10.1096/fj.202002028RR